Crustal anisotropy along the North Anatolian Fault Zone from receiver functions

Andrea Licciardi [1] **(alicciardi@cp.dias.ie**), Tuna Eken [2], Tuncay Taymaz [2], Nicola Piana Agostinetti [1], Seda Yolsal-Çevikbilen [2] and Frederik Tilmann[3,4]

(1) Geophysics Section, School of Cosmic Physics, Dublin Institute for Advanced Studies, Dublin, Ireland (2) Department of Geophysical Engineering, The Faculty of Mines, Istanbul Technical University, Istanbul, Turkey
(3) Deutsches GeoForschungsZentrum GFZ, Potsdam, Germany (4) Freie Universität, Berlin, Germany

EGU2016-8828

Summary

The North Anatolian Fault Zone (NAFZ) that is considered to be one of the largest plate-bounding transform faults separates the Anatolian Plate to the south from the Eurasian Plate to the north. A proper estimation of the crustal anisotropy in the area is a key point to understand the present and past tectonic processes associated with the plate boundary as well as for assessing its strength and stability. In this work we used data from the North Anatolian Fault (NAF) passive seismic experiment in order to retrieve the anisotropic properties of the crust by means of the receiver function (RF) method. This approach provides robust constraints on the location at depth of anisotropic bodies compared to other seismological tools, i.e., S-waves splitting observations where anisotropic parameters are obtained through a path-integrated measurement process over depth.
We computed RFs from teleseismic events, for 39 stations with a recording period of nearly 2 years, providing an excellent azimuthal coverage. The observed azimuthal variations in amplitudes and delay times on the Radial and Transverse RF indicate the presence of anisotropy in the crust. Isotropic and anisotropic effects on the RFs are analyzed separately after harmonic decomposition of the RF dataset (Bianchi et al. 2010). Pseudo 2D profiles are built to observe both the seismic isotropic structure and the depth-dependent lateral variations of crustal anisotropy in the area, including orientation of the symmetry axis. Preliminary results show that the isotropic structure is characterized by a complex crustal setting above a nearly flat Moho at a depth of ~40 km in the central portion of the studied area. Strong anisotropy is present in the upper crust along some portions of the NAFZ and the Ezinepazari-Sungurlu Fault (ESF), with a strong correlation between the orientation of the symmetry axis of anisotropy and the strike of the main geological structures. More complex patterns of anisotropy are present in the middle and lower crust as well as in the upper mantle.

Data

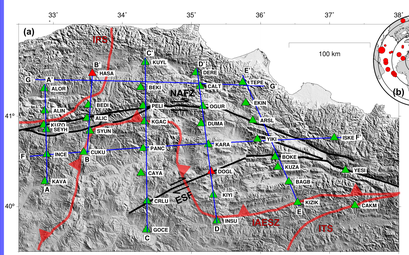

Figure 1. (a) Map with the location of the 38 broadband seismic stations used in this study. Stations belong to the North Anatolian Fault (NAF) passive seismic experiment, which operated from January 2006 to May 2008. Major faults are indicated in black. NAFZ, North Anatolian Fault Zone; ESF, Ezinepazari-Sungurlu Fault. Suture zones modified after Yolsal-Çevikbilen et al. (2012)are indicated in red. IPS, Intra-Pontide Suture; IAESZ, Izmir-Ankara-Erzincan Suture Zone; ITS, Intra-Tauride Suture. Trace of profiles shown in Figure 3 are indicated in blue and labelled. Station used in Figure 2 (HASA and DOGL) are indicated by red triangles. The study area is indicated by a black square. (b) Example of teleseismic events distribution for station DOGL. Red circles indicate selected events with magnitude greater than 5.5 and from epicentral distances between 30° and 100° from which high S/N RF could be computed. With more than 2 years of data, a good backazimuthal coverage is achieved for all the stations considered. (c) Major tectonic units and blocks in Turkey from Okay and Tüysüz (1999).

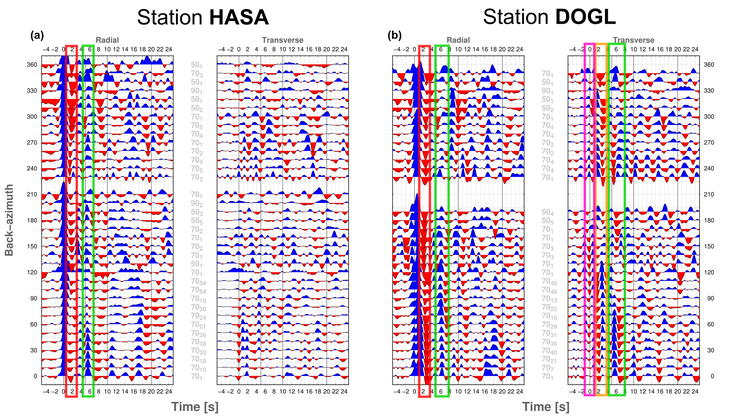

Figure 2. RFs calculated at stations HASA (a) and DOGL (b) (red triangles in Figure 1) sorted as a function of backazimuth. RFs are low-pass filtered with 90% frequency cut-off at ~1Hz. RFs are stacked in backazimuth and epicentral distance bins with width of 20° and 40°, respectively, with 50% overlap. In case of isotropic and flat stratified media only P-to-SV conversions are expected on the Radial component of the RF. Signals on the Transverse component are P-to-SH conversions generated in the presence of anisotropy and/or dipping discontinuities at depth (see Figure 3). The contribution of P-SH conversions is higher at station DOGL than at station HASA.

Results - Profiles

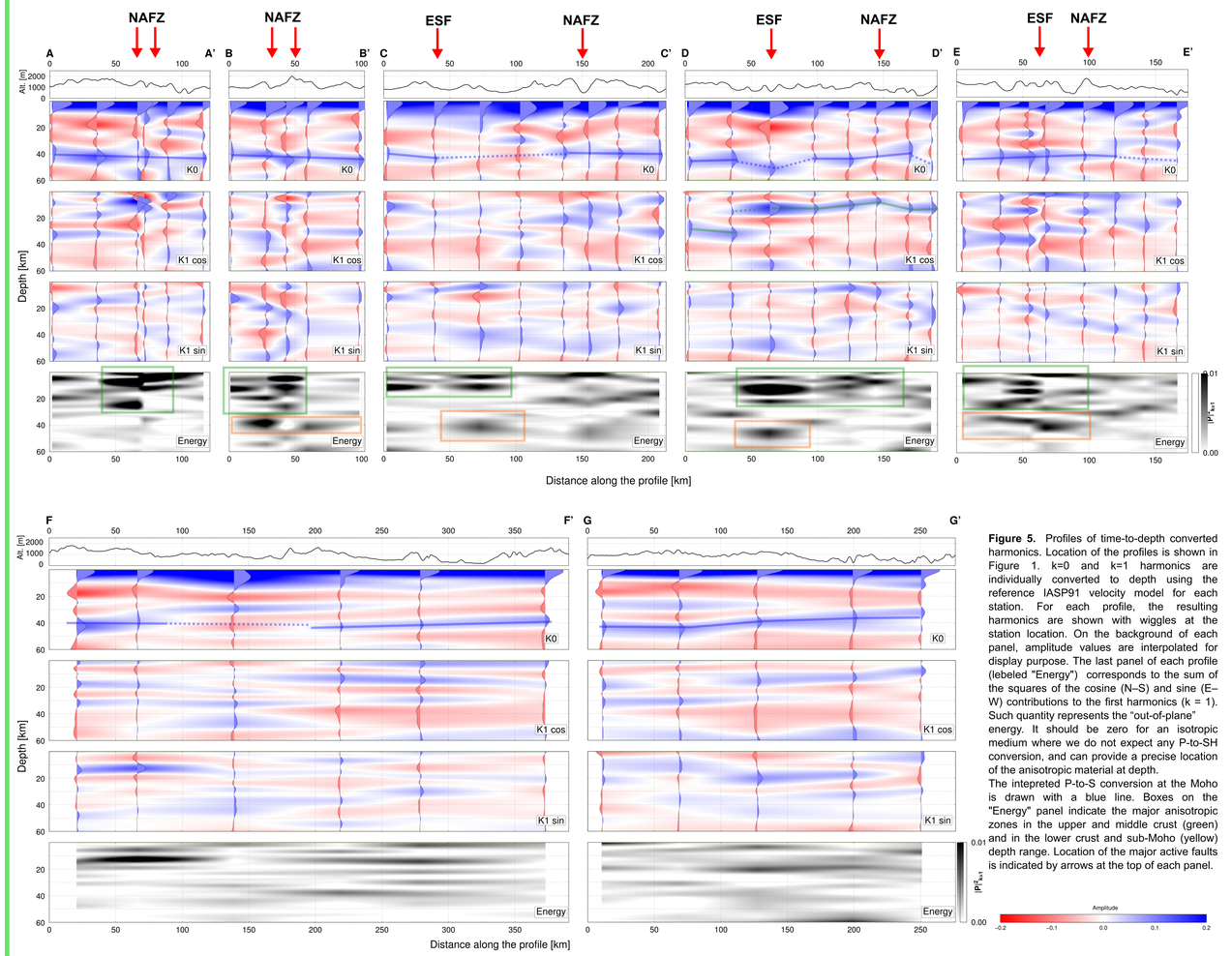

Figure 5. Profiles of time-to-depth converted harmonics. Location of the profiles is shown in Figure 1. k=0 and k=1 harmonics are individually converted to depth using the reference IASP91 velocity model for each station. For each profile, the resulting harmonics are shown with wiggles at the station location. On the background of each panel, amplitude values are interpolated for display purpose. The last panel of each profile (labeled "Energy") corresponds to the sum of the squares of the cosine (N–S) and sine (E–W) contributions to the first harmonics (k = 1). Such quantity represents the "out-of-plane" energy. It should be zero for an isotropic medium where we do not expect any P-to-SH conversion, and can provide a precise location of the anisotropic material at depth.
The intepreted P-to-S conversion at the Moho is drawn with a blue line. Boxes on the "Energy" panel indicate the major anisotropic zones in the upper and middle crust (green) and in the lower crust and sub-Moho (yellow) depth range. Location of the major active faults is indicated by arrows at the top of each panel.

Results - Anisotropy maps

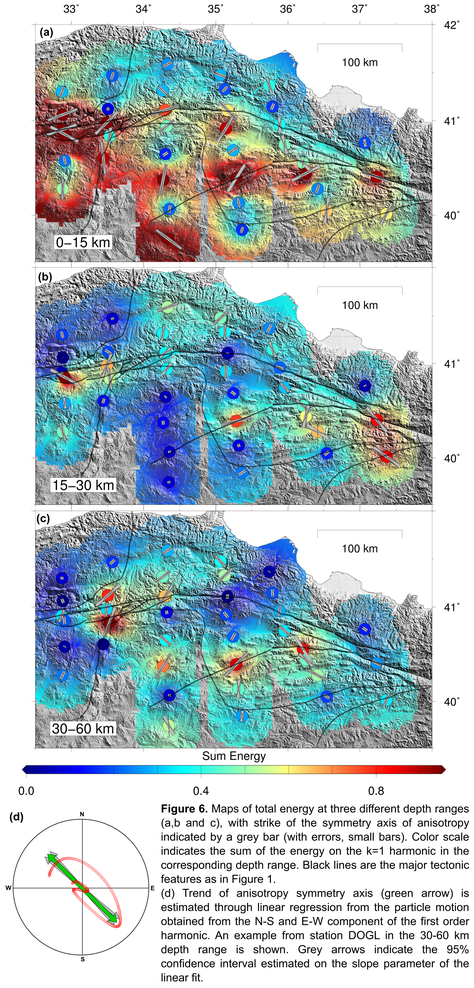

Figure 6. Maps of total energy at three different depth ranges (a,b and c), with strike of the symmetry axis of anisotropy indicated by a grey bar (with errors, small bars). Color scale indicates the sum of the energy on the k=1 harmonic in the corresponding depth range. Black lines are the major tectonic features as in Figure 1.
(d) Trend of anisotropy symmetry axis (green arrow) is estimated through linear regression from the particle motion obtained from the N-S and E-W component of the first order harmonic. An example from station DOGL in the 30-60 km depth range is shown. Grey arrows indicate the 95% confidence interval estimated on the slope parameter of the linear fit.

Anisotropy and harmonic decomposition of RF

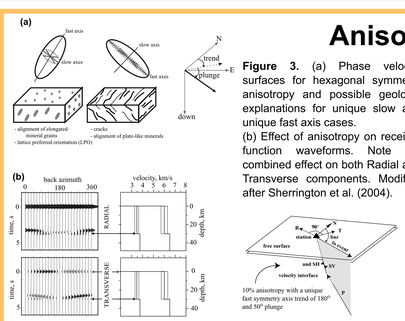

Figure 3. (a) Phase velocity surfaces for hexagonal symmetry anisotropy and possible geologic explanations for unique slow and unique fast axis cases.
(b) Effect of anisotropy on receiver function waveforms. Note the combined effect on both Radial and Transverse components. Modified after Sherrington et al. (2004).

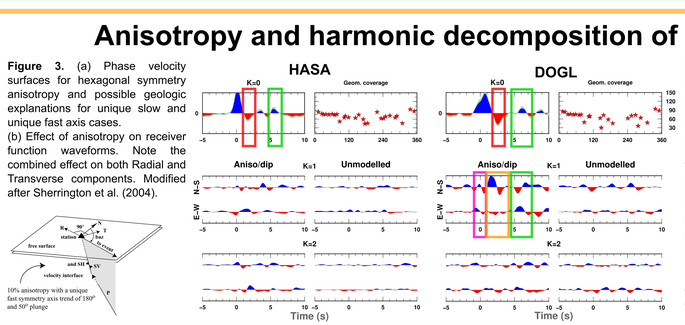

Figure 4. Harmonic decomposition of the RF-dataset at stations HASA and DOGL. The first three order harmonics (k=0,1,2) of each dataset are computed following the method described in Bianchi et al. (2010), to separate the isotropic and anisotropic effects on the RFs. The zero order harmonic is the "constant" term. This represents the backazimuthally invariant response induced by the isotropic and flat stratified medium under the seismic station. The first order harmonics (k=1, on the two perpendicular directions N-S and E-W) contain the energy that shows a 2-lobed periodicity in backazimuth which is due to anisotropic bodies with plunging symmetry axis and/or dipping velocity contrasts. The second order harmonics (k=2) correspond to the signal which possess a 4-lobed periodicity in backazimuth. This is associated with anisotropy with horizontal symmetry axis. The "unmodelled" component for each harmonic order is due to scattering, complex 3D setting and incomplete geometrical coverage Park et al. (2004). In this work, we considered only k=0,1 but non-negligible amount of energy is found also on the k=2 harmincs for many stations in the study area.

Conclusions

1) Small anisotropy north of the NAFZ compared to the south.
2) On the NAFZ, intensity of anisotropy diminishes from W to E.
3) Strong anisotropy on the central and eastern portions of the ESF.
4) High spatial frequency variations in anisotropy intensity occur close to complex fault zones.
5) Strike of anisotropy in the upper crust tends to align with the direction of the main geological structures.
6) Depth-varying orientations of symmetry axis across the crust.

REFERENCES: **Bianchi, I.**, Park, J., Piana Agostinetti, N., Levin, V., 2010. Mapping seismic anisotropy using harmonic decomposition of receiver functions: an application to Northern Apennines, Italy. J. Geophys. Res. 115, B12317. http://dx.doi.org/10.1029/2009JB007061. **Okay, A. &** Tüysüz, O., 1999. Tethyan sutures of northern Turkey, Geol. Soc.London Spec. Pub., 156, 475–515, doi:10.1144/GSL.SP.1999.156.01.22. **Park, J.**, Yuan, H., Levin, V., 2004. Subduction zone anisotropy beneath Corvallis, Oregon: a serpentinite skid mark of trench-parallel terrane migration? J. Geophys. Res. 109. http://dx.doi.org/10.1029/2003JB002718. **Sherrington, H. F.**, G. Zandt, and A. Frederiksen (2004), Crustal fabric in the Tibetan Plateau based on waveform inversion for seismic anisotropy parameters, J. Geophys. Res., 109, B02312, doi:10.1029/2002JB002345. **Yolsal-Çevikbilen, S.**, Biryol, C. B., Beck, S., Zandt, G., Taymaz, T., Adiyaman, H.E., Özacar, A.A., 2012. 3-D crustal structure along the North Anatolian Fault Zone in north-central Anatolia revealed by local earthquake tomography. Geophys. J. Int. 188 (3): 819-849 doi:10.1111/j.1365-246X.2011.05313.x